Design of a Metamaterial-Based Backward-Wave Oscillator

Jason Samuel Hummelt, *Student Member, IEEE*, Samantha M. Lewis, Michael A. Shapiro, *Member, IEEE*, and Richard J. Temkin, *Fellow, IEEE*

***Abstract*— In this paper, we present the design of a microwave generator using metamaterials (MTMs) in a negative index waveguide interacting with a high-power electron beam. The microwave structure is formed by inserting two MTM plates loaded with complementary split-ring-resonators (CSRRs) into a rectangular waveguide. Electromagnetic simulations using the high-frequency structure simulator code confirm the presence of a negative index TM-like mode suitable for use in a backward-wave oscillator (BWO). Particle-in-cell (PIC) simulations using the computer simulation technology (CST) Particle Studio code are performed to evaluate the efficiency of an S-Band MTM-based BWO (MTMBWO) excited by a 500 keV, 80-A electron beam. After about 250 ns, the MTMBWO reaches a saturated output power of 5.75 MW with an efficiency of 14% at a frequency near 2.6 GHz. The MTMBWO is also modeled by representing the MTM plates, which consist of CSRRs, as dielectric slabs whose effective permittivity is given by a Lorentzian model. The dielectric slab model is also simulated with the CST PIC code and shows good qualitative agreement with the simulations including the CSRR loaded plates. A cold test structure was fabricated from brass to test the theoretical predictions of the microwave transmission versus frequency of the negative index waveguide. Test results using a vector network analyzer showed very good agreement with the simulations for the excitation of the negative index TM-like mode near 2.6 GHz. The proposed structure appears to be promising for use in a MTMBWO high-power microwave generator.**

***Index Terms*— Backward-wave oscillator (BWO), metamaterial (MTM), plasma waves, vacuum electronics.**

I. Introduction

METAMATERIALS (MTMs) have unique electromagnetic properties with the potential to open new possibilities in the design of high-power microwave devices. One unique property of MTMs is the ability to support negative index modes due to a simultaneous negative effective permittivity and permeability [1], [2]. Subwavelength resonant structures are used to create macroscopic negative effective parameters. There has been much experimental and theoretical work to investigate the application of these so called double-negative MTMs in various engineering applications, including perfect lens design, electromagnetic cloaking, advanced antenna design, accelerator applications, and coherent microwave generation [3], [4]. Of interest to this paper is the use of MTMs in microwave generation, on which a limited amount of theoretical and experimental work has already been performed [5]–[9]. The challenges faced in the construction of most vacuum electron devices (high-power microwave fields, vacuum environment, frequency tunability, and so on) place unique design considerations on a MTM which are not present in optics or low-power microwave electronics.

The use of high-power electron beams to produce or amplify coherent microwave radiation is a well-established yet active area of research [10]. Traveling wave tubes (TWTs) and backward-wave oscillators (BWOs) are both common types of microwave generators that rely on Cerenkov or Smith–Purcell radiation from an electron beam interacting with a slow wave (phase velocity $v_{\mathrm{ph}} < c$) to produce coherent radiation. While the physical description of both devices is quite similar, the TWT amplifies a microwave signal traveling with the electron beam and the BWO generates a backward wave (group velocity $v_{\mathrm{gr}} < 0$) traveling in the opposite direction of the beam.

Arrays of split-ring resonators (SRRs) were introduced as a means of achieving an effective negative permeability in a bulk material [11]. When used in conjunction with an array of metallic posts, one can create a negative index medium, having simultaneous negative permeability and permittivity. The electric analog of the SRR, the complementary-SRR (CSRR) has been shown to produce a negative permittivity [12]. In addition, a TM mode in a below-cutoff waveguide is equivalent to a negative effective permeability medium. To create a waveguide that supports a negative index mode, we propose the use of CSRRs in a below-cutoff waveguide. Since a TM mode is of interest for interacting axially with an electron beam, two parallel CSRR plates running along the electron beam trajectory are used. The geometrical arrangement of the MTM layers is shown to affect the properties of the modes they support, which has also been discussed in [13].

In a mode with negative dispersion, power flows antiparallel to the electron beam's motion. While the interaction is similar in nature to a traditional BWO, it is unique in that a conventional BWO relies upon the interaction of an electron beam with spatial harmonics of a slow-wave structure. In a negative index guide, a mode with negative group velocity is supported by the simultaneous negative permittivity and permeability

Manuscript received December 16, 2013; revised February 7, 2014; accepted February 19, 2014. Date of publication March 25, 2014; date of current version April 8, 2014. This work was supported by AFOSR MURI under Grant FA9550-12-1-0489 through the University of New Mexico, Albuquerque, NM, USA.

The authors are with the Plasma Science and Fusion Center, Massachusetts Institute of Technology, Cambridge, MA 02139 USA (e-mail: hummelt@mit.edu; lewissamim@gmail.com; shapiro@psfc.mit.edu; temkin@mit.edu).

Color versions of one or more of the figures in this paper are available online at http://ieeexplore.ieee.org.

Digital Object Identifier 10.1109/TPS.2014.2309597

0093-3813 © 2014 IEEE. Personal use is permitted, but republication/redistribution requires IEEE permission.
See http://www.ieee.org/publications_standards/publications/rights/index.html for more information.

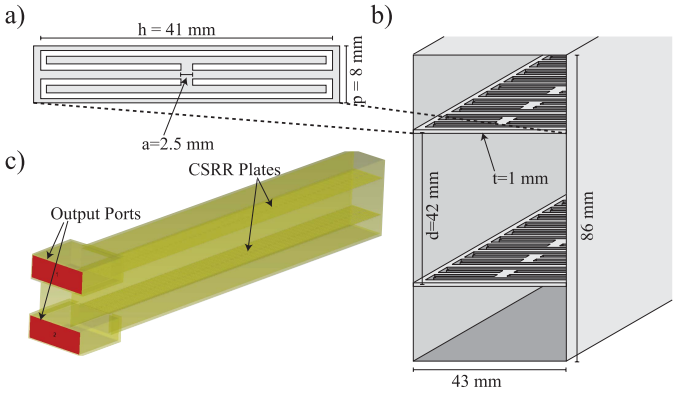

Fig. 1. (a) Simplified schematic of one period of CSRR MTM plate. (b) Simplified schematic of MTMBWO waveguide. CSRRs are machined into two metal plates of thickness $t = 1$ mm and inserted into a standard size WR340 waveguide with a separation of $d = 42$ mm. The CSRRs have period $p = 8$ mm and width $h = 41$ mm. (c) Semitransparent view of total structure including output coupling, created by mating WR284 waveguide to the MTMBWO.

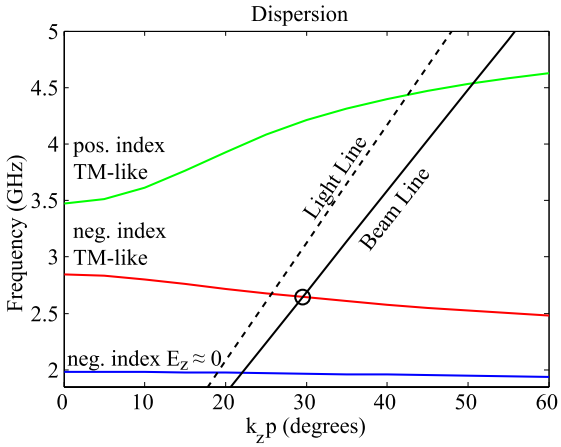

Fig. 2. Dispersion relation for one period of the MTMBWO shown in Fig. 1. The frequency of the BWO interaction for the negative index TM-like mode predicted by HFSS is 2.65 GHz.

of the guide. A related approach in creating structures that support modes with negative group velocity makes use of plasmonic waveguides [14]–[19]. The use of MTMs in a waveguide provides a means to artificially duplicate the dispersive effect of the plasma without creating the problem of actually producing and sustaining a plasma in a microwave tube.

A major motivation of the present study is the understanding of the physical principles of the operation of an MTM-based vacuum electron device. In addition, MTM devices may have some advantages over conventional slow-wave vacuum electron devices. The MTM structure proposed here is a planar structure formed as a metal plate. Large scale manufacturing of a device with planar (2-D) elements is inherently simpler and easier to fabricate than a structure that has a 3-D interaction slow-wave structure, such as coupled cavities. Another potential advantage of the MTM device is its operation in a waveguide below cutoff, which allows the transverse dimensions of the structure to be much smaller than a wavelength. This is important in the miniaturization of low frequency (<10 GHz) microwave generators and amplifiers where structure size can be a limiting factor. Further miniaturization could be achieved using alternative MTM elements.

II. Structure Design and Electromagnetic Simulations

In Fig. 1, we show a specific design for a proposed MTM-based BWO (MTMBWO) structure that will operate in S-Band (2–4 GHz). Other frequency devices can also be designed by scaling the structure shown. The MTMBWO is constructed by placing two periodic MTM plates into a rectangular waveguide. Schematics of one period of the MTM plate and of the structure are shown in Fig. 1(a) and (b), respectively. The resonant frequency of the MTM plates is designed to be below cutoff for TM modes in the waveguide. The MTM plates are created by machining CSRRs with period $p = 8$ mm and width $h = 41$ mm along two metal plates of thickness $t = 1$ mm. The resonators have a slot width of $a = 2.5$ mm. These plates are then placed with a separation of $d = 42$ mm in a standard size WR340 waveguide (inner dimensions 86 mm × 43 mm). In Fig. 1(c), a structure is shown with output coupling included, which is WR284 (inner dimensions 76 mm × 34 mm) waveguide mated to the MTMBWO structure. The overall length of the structure is 440 mm. The cutoff frequency, f_c, of the lowest order TM mode in a rectangular waveguide of transverse dimensions $l_1 \times l_2$ is given by the relation

$$f_c = \frac{1}{2\pi\sqrt{\epsilon_0\mu_0}}\sqrt{\frac{\pi^2}{l_1^2}+\frac{\pi^2}{l_2^2}} \tag{1}$$

where ϵ_0 and μ_0 are the free space permittivity and permeability, respectively. For an empty 43 mm × 86 mm rectangular waveguide $f_c = 3.90$ GHz.

The eigenmode solver of the high-frequency structure simulator (HFSS) code is used to simulate the eigenmodes of one period of the total structure. The eigenmode simulations also generate 3-D E and H field vectors in the structure, which can be used to estimate BWO performance parameters (coupling impedance, start current, and so on) [20], [21]. Because of symmetry along the center of the structure in the plane parallel to the CSRR plates, a perfect-H boundary was used to reduce simulation time. In Fig. 2, the dispersion relation calculated from the HFSS simulation is shown, along with both the beam line $2\pi f = k_z v_0$ and the light line $2\pi f = k_z c$. Here, $2\pi f$ is the angular frequency, c is the speed of light, k_z is the wavenumber, and $v_0 = 0.86\ c$ is the velocity of a 500-keV electron. The structure supports two negative index modes, one with $E_z \approx 0$ at the axis at ~2 GHz and a TM-like ($H_z = 0$ at the axis) at ~2.5 GHz. Because the axial field is small, the negative index mode at 2 GHz is not expected to interact strongly with the electron beam and is also not observed in particle-in-cell (PIC) simulation. The beam line intersects the dispersion relation for the negative index TM-like mode at approximately 2.65 GHz, where the group velocity $v_{\rm gr} \equiv \partial\omega/\partial k < 0$ and the phase velocity $v_{\rm ph} \equiv \omega/k > 0$. The magnitude of the group velocity of

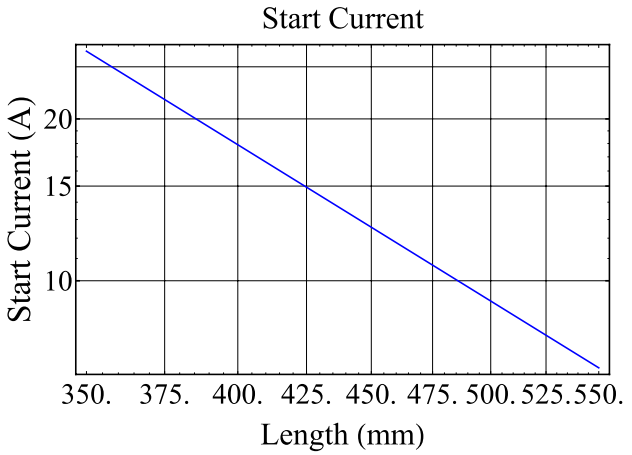

Fig. 3. Start current as a function of total structure length for the design shown in Fig. 1.

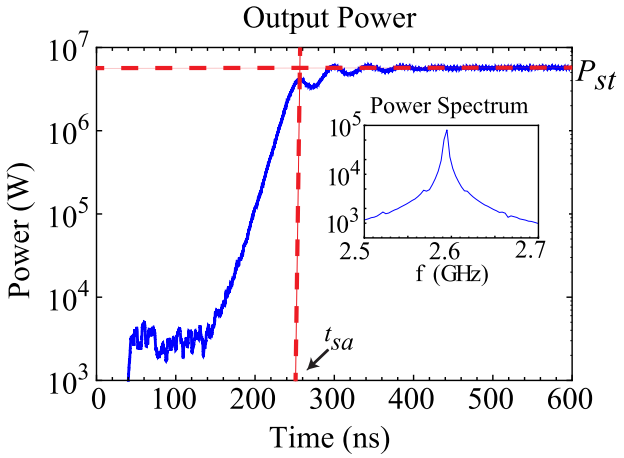

Fig. 4. Output power as a function of time for 80 A in a structure of length 438 mm. Here, $t_{sa} = 258$ ns is the saturation time of the structure and $P_{st} = 5.75$ MW defines the stationary power output. The Fourier transform of the output signal after saturation is reached is shown in the inset.

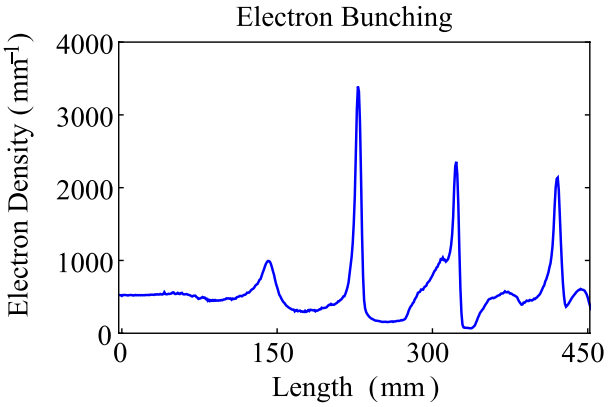

Fig. 5. Plot of electron density showing the formation of axial bunches at $\lambda_z \approx 9$ cm. The electron density shown is taken 400 ns after the injection of the electron beam, i.e., the device has reached saturation.

the negative index TM-like mode at the point of intersection with the beam line is $|v_{gr}| \approx 0.075\ c$.

Of particular interest is the performance of the MTMBWO when compared against a more conventional BWO, such as a rippled wall device. In such a microwave generator there is a start current for oscillation, I_{st}, above which the device will oscillate with zero input signal. The start current depends on the device geometry, mode of interaction, and beam parameters. Traditionally, one operates the BWO at $\sim 3\times$ the start current. Increasing the current well beyond the start current ($>7\times$) can result in automodulation of the output power as the device enters a stochastic regime. This type of behavior has been observed in both theory and experiment, as shown, for example, in [22]. To estimate the start current for the MTMBWO, we use a loss-less linear theory outlined in [21]. The coupling impedance is given by the relation

$$Z = \frac{|E_w|^2}{2k_{z0}^2 P} \tag{2}$$

where $|E_w|$ is the component of the electric field parallel to the direction of and in phase with the electron beam, P is the power flux, and k_{z0} is the wavenumber. The numerical value of the coupling impedance is calculated from the electric and magnetic field profiles generated by the HFSS eigenmode simulation for the negative index TM-like mode and is found to be $Z = 46\ \Omega$. The start current is then readily calculated from

$$I_{st} = 4U_0 \frac{(CN)_{st}^3 \lambda_z^3}{ZL^3} \tag{3}$$

where U_0 is the beam energy, $\lambda_z = 2\pi/k_z$ is the longitudinal wavelength (9.6 cm), L is the total length of the structure, $N = L/\lambda_z$ is the number of longitudinal wavelengths, and C is the Pierce parameter given by

$$C^3 = \frac{I_0 Z}{4U_0}. \tag{4}$$

Here, I_0 is the beam current. From [21, Table 8.1], the start condition $(CN)_{st}$ is taken to be 0.314 for zeroth-order axial harmonic operation. From (3), the start current is plotted in Fig. 3 as a function of structure length.

III. PIC-Simulation Results and Discussion

We use the PIC solver of computer simulation technology (CST) Particle Studio to investigate the performance of the MTMBWO utilizing a relativistic electron beam. A variable current (60, 80, and 100 A) and a 500 keV ($v_0 = 0.86\ c$) beam of radius 2.2 mm is used for the simulations. The electron beam simulated was a dc beam with a 4 ns rise time to reach full current from zero initial starting current. A uniform and axial magnetic field of 1.5 kG is used for all simulations. Output ports are shown in Fig. 1(c) and were used to record the power generated and coupled out of the structure.

Fig. 4 shows the output power as a function of time for a simulation of a 438-mm long MTMBWO structure using an 80-A electron beam. The device takes 260 ns to reach a stationary output power regime where 5.75-MW average power was produced at 2.595 GHz. Shown in Fig. 5 is a plot of the electron density for the same simulation taken at 400 ns that clearly demonstrates the formation of electron bunches in the device. As the bunches travel along the axis, they start to break up as they lose energy to the wave and due to space charge.

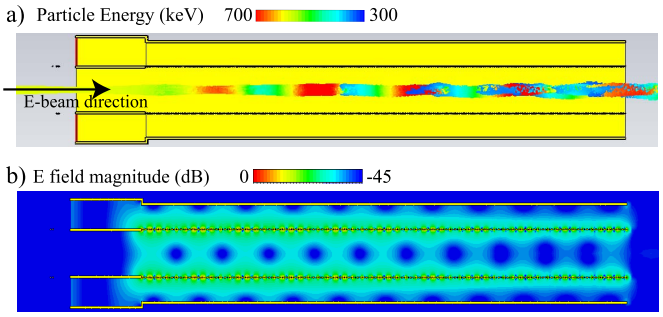

Fig. 6. (a) Cross section of the MTMBWO showing particle trajectories for a 438-mm long structure. The individual energy of each particle is indicated by the color scale. (b) Electric field magnitude in the MTMBWO. Both snapshots are taken 400 ns after the injection of the electron beam, i.e., the device has reached saturation.

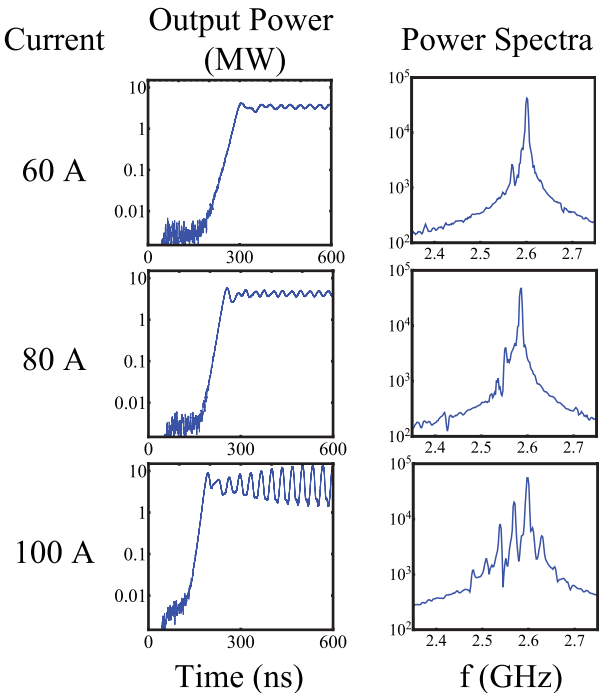

Fig. 7. Output powers and power spectra of stationary outputs for currents of 60, 80, and 100 A. The structure length for all three simulations was 462 mm.

A plot of the electron trajectories is shown in Fig. 6(a). This plot is also from the same simulation and taken at 400 ns. The energy of individual particles is indicated by their color, and distinct electron bunches are visible. The beam size is affected by the RF field and a slight increase in the beam radius is visible as the beam exits the MTMBWO structure. The electric field magnitude at this time is shown in Fig. 6(b). The field grows from zero at the electron beam exit to its peak value at the beam entrance, indicating the backwardness of the mode. The field strength is greatest close to the MTM plates.

In Fig. 7, the output power and spectrum are shown for a 60, 80, and 100 A beam for a fixed length of 462 mm. Using the results of (3) and Fig. 3, the nominal start current for the MTMBWO is 12 A for a 462-mm long structure. A clear change in the behavior of the MTMBWO is visible as the current is increased from 80 to 100 A, corresponding to

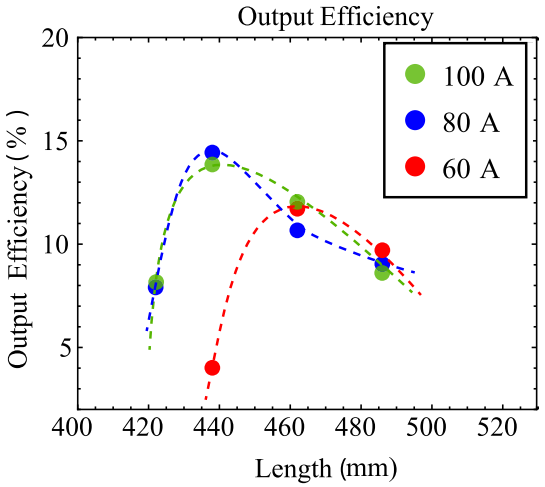

Fig. 8. Output efficiency versus structure length for $I = 60$, 80, and 100 A. Dashed lines are included as a guide for the eye.

6.7 and 8.3 times the start current, respectively. At 100 A there is automodulation of the output power, which is indicated by the multifrequency operation in the output spectra. Note that for an interaction length of 438 mm and a beam current of 80 A the automodulation instability is absent, which is shown in Fig. 4.

Output efficiency is an important figure of merit when comparing the MTMBWO against more traditional BWO designs. The output efficiency, calculated by taking the average steady-state power output at the output ports divided by the beam power is shown in Fig. 8 as a function of structure length for three different beam currents. A peak efficiency of 14.5% is predicted for the 438-mm long structure using 80 A.

IV. Effective Medium PIC-Simulation Results and Discussion

A standard and convenient way to interpret the dispersive qualities of a MTM is by use of an effective medium model, which treats the collective electromagnetic behavior of individual MTM resonators as a bulk material with an effective permittivity or permeability [23]. Comparison between such a model and actual MTM resonators can verify that the resonators are indeed acting as a MTM (i.e., providing an effective negative permittivity or permeability at the frequency of interest). More practically, the simulation of a MTM using a PIC code can be computationally intensive, as accurately meshing the subwavelength resonators can make for extremely large mesh sizes. Thus substituting the actual MTM resonators with a bulk material can save simulation time. A similar approach to simulate a MTM interacting with an electron beam using an effective medium was used in [5].

We again use the PIC solver in CST Particle Studio to simulate a MTM-based BWO similar to the MTMBWO investigated in the previous section. Instead of using CSRR-based MTM plates, an isotropic effective medium is inserted into the waveguide which models the dispersive qualities of the CSRRs. The model is shown in Fig. 9, where the same outer waveguide as the MTMBWO (WR340) is used to provide a

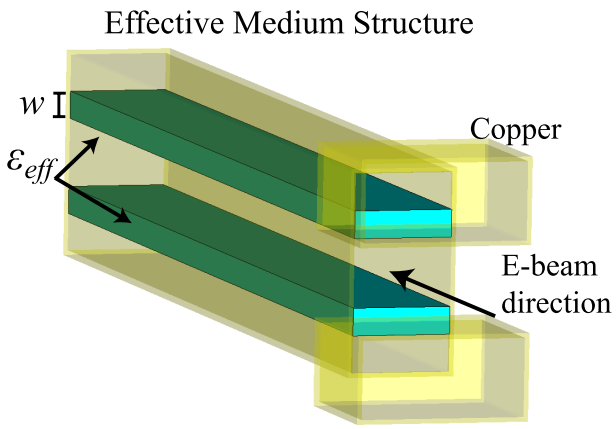

Fig. 9. Effective medium BWO. The device is identical to the MTMBWO introduced in the previous section, but the CSRR plates have been replaced by an isotropic dielectric slab of width $w = 12$ mm and permittivity modeled by (6).

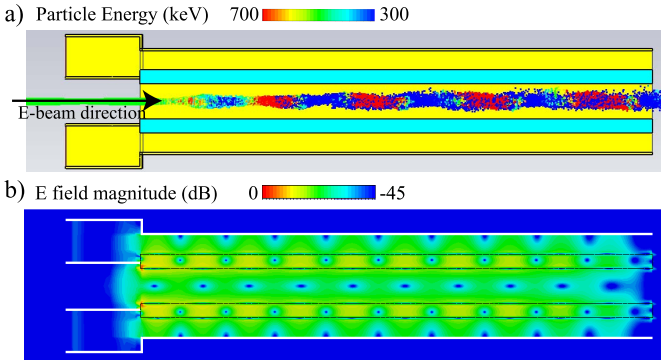

Fig. 10. (a) Cross section of the effective medium BWO showing particle trajectories for a 438-mm long structure. The individual energy of each particle is indicated by the color scale. Note the qualitative similarity to Fig. 6(a). (b) Electric field magnitude in the effective medium BWO. Both snapshots are taken 700 ns after the injection of the electron beam, i.e., the device has reached saturation.

negative permeability. Using the Drude model, the permeability of a waveguide follows the expression [3], [24]:

$$\mu_{\text{eff}} = 1 - \frac{\omega_c^2}{\omega^2} \tag{5}$$

where $\omega_c = 2\pi \cdot 3.90$ GHz is the cutoff frequency of the fundamental TM mode, and the numerical value was calculated for the WR340 waveguide using (1). For $\omega < \omega_c$, the permeability of the waveguide is negative.

Coupling power out of the structure is identical in both the effective medium model and MTMBWO. Two dielectric slabs of width $w = 12$ mm are placed in the same location as the CSRR loaded plates in the MTMBWO. The overall length of the structure is $L = 438$-mm long. The electron beam parameters used, $I = 80$ A, $U_0 = 500$ keV, and beam radius $r_b = 2.2$ mm, are consistent with those used in the simulations of the MTMBWO. A Lorentz model for the dispersion of the effective medium is used, which is given by the relation [3], [24]

$$\epsilon_{\text{eff}} = 1 - \frac{\omega_p^2}{\omega^2 - \omega_0^2} \tag{6}$$

where ω_p is the plasma frequency and ω_0 is the resonant frequency of the CSRRs. The particular numerical values are chosen for these two frequencies from the dispersion relation obtained by the HFSS eigenmode solver to mimic the dispersion of the MTMBWO. Since the permittivity is given by $\epsilon = c^2k^2/\omega^2$, the resonance and plasma frequencies in (6) are determined from the dispersion relation (shown in Fig. 2) by letting $\epsilon \to \infty$ and $\epsilon \to 0$, which corresponds to letting $k_z p \to \infty$ and $k_z p \to 0$, respectively. We find the resonance to be at $\omega_0 = 2\pi \cdot 2.3$ GHz and the plasma frequency is determined to be $\omega_p = 2\pi \cdot 1.7$ GHz.

Fig. 10(a) shows the particle trajectories and formation of electron bunches due to the BWO interaction. The magnitude of the electric field is displayed in Fig. 10(b). Comparing this with the fields shown for the CSRR-based MTMBWO in Fig. 6(b), we see a similar field structure in the region of the

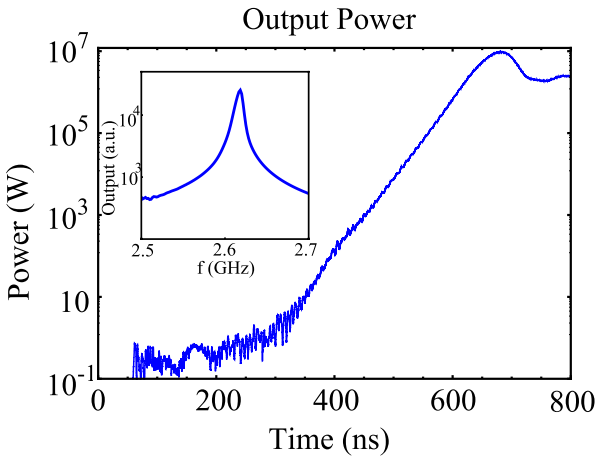

Fig. 11. Output power and power spectrum of the full output signal for the structure in Fig. 9. The structure simulated was 438-mm long. The effective medium operation frequency of 2.62 GHz is close to the actual MTMBWO structure of the same length at 2.595 GHz.

guide outside of the dielectric slab (i.e., in the beam tunnel and above and below the slab). The output power as a function of time and the Fourier transform of this signal is given in Fig. 11. The device saturates at 3 MW and the frequency is 2.62 GHz, which is near the output frequency of the MTMBWO of the same length at 2.595 GHz and approximately half of the saturated power. Different slab widths w were investigated, with 3 to 20 mm having a similar frequency response with some variation in output power and saturation time. For $w = 1$ mm the slab was too thin for the beam to couple to the guide, and as the slab was made very large (>20 mm) the presence of the slab interfered with power coupling out of the guide. As the slab thickness has been shown to be important in the overall response of MTM layers, a more detailed analysis would be necessary to determine exact slab parameters to replicate the CSRR loaded plates [25]. Although the results of the analysis provided by this model are not in exact agreement with the exact MTMBWO structure, they do provide valuable physical insight [26].

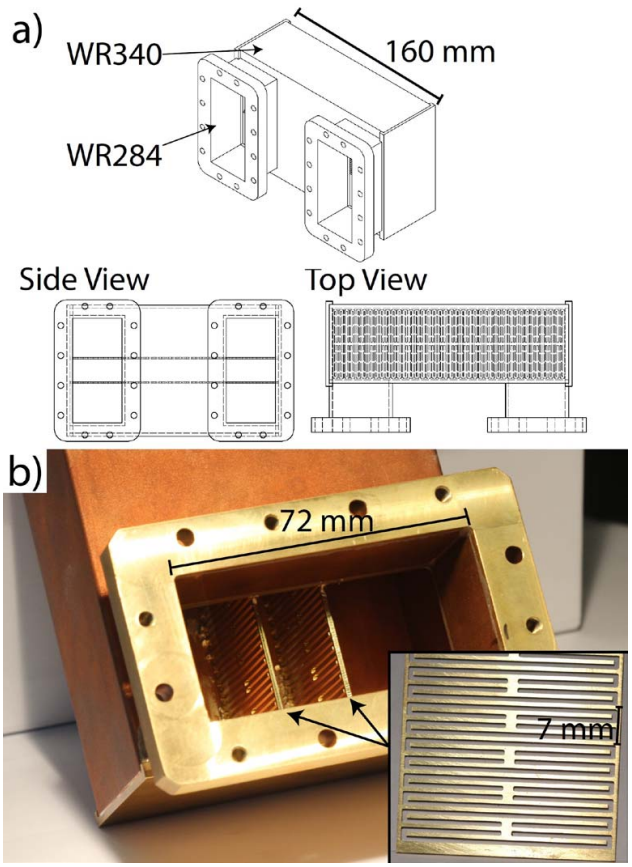

Fig. 12. (a) Schematics and (b) photograph of test structure and CSRR loaded thin brass plate. The photo is taken looking into one of the identical WR284 input ports for coupling in/out of the structure. The negative index mode in the test CSRR structure is excited by the fundamental mode of the input WR284 waveguide.

V. Structure Cold Test Results

To validate the electromagnetic response of the MTMBWO design, measurements of microwave transmission in a test MTMBWO structure made of brass were performed using a vector network analyzer (VNA). Experimental measurements of various coupling schemes to MTM devices has been investigated due to the importance for real-world MTMs [27], [28]. The test structure and schematics are shown in Fig. 12. The structure is identical to that shown in Fig. 1 except with $p = 7$ mm, $d = 16$ mm, and $a = 2$ mm. The overall structure length was 20 periods (160 mm). The MTM plates were aligned in the WR340 waveguide by end supporting plates, and the MTM resonators were created by machining out two brass plates. Coupling to the negative index mode was nontrivial since the electric field topology of the negative index mode in the MTMBWO is unlike the fundamental waveguide mode.

Several coupling designs were investigated to try and minimize reflection near the operation frequency. In this test design, coupling was accomplished through WR284 waveguide mated to the side of the MTMBWO test structure. This matched the polarization of electric field in the fundamental TE mode of the WR284 waveguide and the polarization of the axial field in the negative index TM-like mode of the MTMBWO test structure. This coupling scheme is different

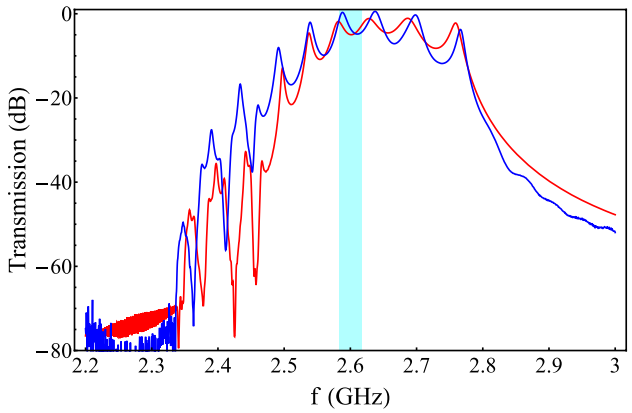

Fig. 13. Transmission measurement of the test MTMBWO structure (blue) compared with CST Microwave Studio simulation (red). The planned operation frequency band is highlighted in light blue.

than that used in the PIC simulations of the MTMBWO, and was chosen for simplicity of design. Coax to WR284 waveguide adapters are used to excite the fundamental TE mode in the WR284 waveguide. The transmission measurement is shown in Fig. 13 in blue, along with a simulation of the same setup using CST Microwave Studio in red. Excitation of the negative index mode is demonstrated by nonzero transmission where the negative index mode was predicted by HFSS eigenmode simulation. The planned operation frequency of the MTMBWO near 2.6 GHz is highlighted in light blue.

VI. Conclusion

The design of a microwave generator using MTMs in a negative index waveguide has been presented. The potential benefits of a MTM-based microwave generator over conventional sources has been discussed, including increased manufacturability and miniaturization. HFSS eigenmode simulations have been presented to confirm the presence of the negative index mode and estimate coupling to the beam. The device operates as a BWO with the negative index mode supported by the MTM plates. CST PIC simulations have been used to demonstrate the performance of the device in use with a 500 keV and 60–100-A electron beam. Efficiency of >14% is observed with saturated output of 5.75 MW at 500 keV, 80-A operation. An effective medium model is presented, which models the MTM as a dielectric with a Lorentzian response. The model structure is also simulated with the CST PIC code and the output power and frequency are in qualitative agreement with the full MTM PIC simulations. Finally, to verify the electromagnetic design of the MTM device a test structure was designed and tested using a VNA, and transmission measurements confirmed the presence and excitation of the negative index mode.

References

[1] D. R. Smith, W. J. Padilla, D. C. Vier, S. C. Nemat-Nasser, and S. Schultz, "Composite medium with simultaneously negative permeability and permittivity," *Phys. Rev. Lett.*, vol. 84, no. 18, pp. 4184–4187, 2000.

[2] D. R. Smith and N. Kroll, "Negative refractive index in left-handed materials," *Phys. Rev. Lett.*, vol. 85, no. 14, pp. 2933–2936, 2000.

[3] R. Marques, F. Martin, and M. Sorolla, *Metamaterials with Negative Parameters: Theory, Design and Microwave Applications*. Hoboken, NJ, USA: Wiley, 2008.
[4] L. Solymar and E. Shamonina, *Waves in Metamaterials*. New York, NY, USA: Oxford Univ. Press, 2009.
[5] Y. P. Bliokh, S. Savel'ev, and F. Nori, "Electron beam instability in left-handed media," *Phys. Rev. Lett.*, vol. 100, no. 4, p. 244803, 2008.
[6] A. Antipov *et al.*, "Observation of wakefield generation in left-handed band of metamaterial-loaded waveguide," *J. Appl. Phys.*, vol. 104, no. 1, pp. 014901-1–014901-6, 2008.
[7] D. Shiffler, J. Luginsland, D. M. French, and J. Watrous, "A Cerenkov-like maser based on a metamaterial structure," *IEEE Trans. Plasma Sci.*, vol. 38, no. 6, pp. 1462–1465, Jun. 2010.
[8] M. A. Shapiro, S. Trendafilov, Y. Urzhumov, A. Alu, R. J. Temkin, and G. Shvets, "Active negative-index metamaterial powered by an electron beam," *Phys. Rev. B*, vol. 86, no. 8, p. 085132, 2012.
[9] D. M. French, D. Shiffler, and K. Cartwright, "Electron beam coupling to a metamaterial structure," *Phys. Plasmas*, vol. 20, no. 8, p. 083116, 2013.
[10] S. H. Gold and G. S. Nusinovich, "Review of high-power microwave source research," *Rev. Sci. Instrum.*, vol. 68, no. 11, pp. 3945–3974, 1997.
[11] J. B. Pendry, A. J. Holden, D. J. Robbins, and W. J. Stewart, "Magnetism from conductors and enhanced nonlinear phenomena," *IEEE Trans. Microw. Theory Tech.*, vol. 47, no. 11, pp. 2075–2084, Nov. 1999.
[12] F. Falcone *et al.*, "Babinet principle applied to the design of metasurfaces and metamaterials," *Phys. Rev. Lett.*, vol. 93, no. 19, p. 197401, 2004.
[13] G. Shvets, "Photonic approach to making a material with a negative index of refraction," *Phys. Rev. B*, vol. 67, no. 3, p. 035109, 2003.
[14] A. W. Trivelpiece and R. W. Gould, "Space charge waves in cylindrical plasma columns," *J. Appl. Phys.*, vol. 30, no. 11, pp. 1784–1793, 1959.
[15] V. N. Shevchik, G. N. Shvedov, and A. V. Soboleva, *Wave and Oscillatory Phenomena in Electron Beams at Microwave Frequencies*. Oxford, U.K.: Pergamon Press, 1966.
[16] Y. Carmel *et al.*, "Demonstration of efficiency enhancement in a high-power backward-wave oscillator by plasma injection," *Phys. Rev. Lett.*, vol. 62, no. 20, pp. 2389–2392, 1989.
[17] A. T. Lin and L. Chen, "Plasma-induced efficiency enhancement in a backward-wave oscillator," *Phys. Rev. Lett.*, vol. 63, no. 26, pp. 2808–2811, 1989.
[18] A. G. Shkvarunets *et al.*, "Operation of a relativistic backward-wave oscillator filled with a preionized high-density radially inhomogeneous plasma," *IEEE Trans. Plasma Sci.*, vol. 26, no. 3, pp. 646–652, Jun. 1998.
[19] C. Grabowski, J. M. Gahl, and E. Schamiloglu, "Initial plasma-filled backward-wave oscillator experiments using a cathode-mounted plasma prefill Source," *IEEE Trans. Plasma Sci.*, vol. 26, no. 3, pp. 653–668, Jun. 1998.
[20] M. Aloisio and P. Waller, "Analysis of helical slow-wave structures for space TWTs using 3-D electromagnetic simulations," *IEEE Trans. Electron Devices*, vol. 52, no. 5, pp. 749–754, May 2005.
[21] S. E. Tsimring, *Electron Beams and Microwave Vacuum Electronics*. Hoboken, NJ, USA: Wiley, 2007.
[22] N. S. Ginzburg *et al.*, "Observation of chaotic dynamics in a powerful backward-wave oscillator," *Phys. Rev. Lett.*, vol. 89, no. 10, p. 108304, 2002.
[23] T. Koschny, E. N. Economou, and C. M. Soukoulis, "Effective medium theory of left-handed materials," *Phys. Rev. Lett.*, vol. 93, no. 10, p. 107402, 2004.
[24] J. Esteban, C. Camacho-Penalosa, J. E. Page, T. M. Martin-Guerrero, and E. Marquez-Segura, "Simulation of negative permittivity and negative permeability by means of evanescent waveguide modes-theory and experiment," *IEEE Trans. Microw. Theory Tech.*, vol. 53, no. 4, pp. 1506–1514, Apr. 2005.
[25] C. L. Holloway, E. F. Kuester, J. A. Gordon, J. O'Hara, J. Booth, and D. R. Smith, "An overview of the theory and applications of metasurfaces: The two-dimensional equivalents of metamaterials," *IEEE Antennas Propag. Mag.*, vol. 54, no. 2, pp. 10–31, Apr. 2012.
[26] T. Koschny, P. Markos, E. N. Economou, D. R. Smith, D. C. Vier, and C. M. Soukoulis, "Impact of inherent periodic structure on effective medium description of left-handed and related metamaterials," *Phys. Rev. B*, vol. 71, no. 4, p. 245105, 2005.
[27] R. Liu *et al.*, "Experimental demonstration of electromagnetic tunneling through an epsilon-near-zero metamaterial at microwave frequencies," *Phys. Rev. Lett.*, vol. 100, no. 2, p. 023903, 2008.
[28] B. Edwards, A. Alu, M. E. Young, M. Silveirinha, and N. Engheta, "Experimental verification of epsilon-near-zero metamaterial coupling and energy squeezing using a microwave waveguide," *Phys. Rev. Lett.*, vol. 100, no. 3, p. 033903, 2008.

Jason Samuel Hummelt (S'12) received the B.S. degree in nuclear engineering and physics and the M.S. degree in engineering physics from the University of Wisconsin-Madison, Madison, WI, USA. He is currently pursuing the Ph.D. degree with the Massachusetts Institute of Technology, Cambridge, MA, USA.

He has been with the Plasma Science and Fusion Center, Massachusetts Institute of Technology, since 2010. His current research interests include high-power microwave and laser breakdown both in air and vacuum, microwave generation, metamaterials, photonic bandgap structures, and various millimeter-wave applications.

Samantha M. Lewis is currently pursuing the Degree in nuclear science and engineering with the Massachusetts Institute of Technology, Cambridge, MA, USA.

She has been with the Plasma Science and Fusion Center, Massachusetts Institute of Technology, since 2012. Her current research interests include high-power microwave generation, microwave applications, and metamaterials.

Michael A. Shapiro (M'09) received the Ph.D. degree in radio physics from the University of Gorky, Gorky, Russia, in 1990.

He has been with the Plasma Science and Fusion Center, Massachusetts Institute of Technology, Cambridge, MA, USA, since 1995, where he is currently the Head of the Gyrotron Research Group. His current research interests include vacuum microwave electron devices, high-power gyrotrons, dynamic nuclear polarization spectroscopy, high-gradient linear accelerators, quasi-optical millimeter-wave components, and photonic bandgap structures and metamaterials.

Richard J. Temkin (M'87–SM'92–F'94) received the B.A. and Ph.D. degrees in physics from Harvard College, Cambridge, MA, USA, and the Massachusetts Institute of Technology (MIT), Cambridge.

He was a Post-Doctoral Research Fellow with the Division of Engineering and Applied Physics, Harvard University, Cambridge, from 1971 to 1974. Since 1974, he has been with MIT, first with the Francis Bitter National Magnet Laboratory and later with the Plasma Science and Fusion Center (PSFC) and the Department of Physics. He currently serves as a Senior Scientist with the Physics Department, as an Associate Director at PSFC, and the Head of the Waves and Beams Division, PSFC. He has been the author and co-author of more than 200 published journal articles and book chapters, and has been the Editor of six books and conference proceedings.

Dr. Temkin is a fellow of the American Physical Society and the Institute of Physics, London, U.K. He has been the recipient of the IEEE Plasma Science and Applications Award, the Kenneth J. Button Prize and Medal, the Robert L. Woods Award of the Department of Defense, the Exceptional Service Award from the International Society of Infrared, Millimeter, and Terahertz Waves, a Certificate of Merit from the U.S. Department of Energy, and a Certificate of Recognition from the IEEE Electron Device Society.